Finite Element Simulation of 2-D Rayleigh-Benard-Marangoni Problems

Ph.D Thesis Proposal

Andréa M. P. Valli

December, 1998

Adviser: *Álvaro L.G.A. Coutinho*

Co-adviser: *Graham F. Carey*

Contents

Chapter 1

Introduction

Natural convection of an incompressible fluid can be driven by buoyancy forces due to temperature gradients and thermocapillary forces caused by gradients in the surface tension. When a thin horizontal layer fluid between two horizontal plates is heated from below, a temperature gradient is generated across the plates. At critical Rayleigh number, circular convection cells set in - the heated fluid near the bottom begins to rise while the cooler fluid near to the top descends. Buoyancy is a dominant component in driving this type of flow termed Rayleigh-Benard problem [10, 9, 7]. If the plate is removed from the upper surface, then the surface tension effects associate with temperature gradients on the free surface become important [16, 6, 21]. Now both buoyancy and thermocapillary effects provide the dominant forces driving the flow. These flows are termed Rayleigh-Benard-Marangoni problems.

Coupled viscous flow and heat transfer computations are of great interest in studying pattern formation in hydrodynamical systems. Practical applications include, for example, pattern formation during solidification, welding in manufacturing processes and growth phenomena to defect fracture and crack propagation [19, 5, 16]. Rayleigh-Benard-Marangoni problems become very popular as prototypes of complex behavior where nonlinear theories of pattern formation may be tested. Recently, special attention has been paid to the study and implementation of numerical and computational techniques to develop effective algorithms capable of high resolution 3D viscous flows involving heat transfer and surface tension effects. For example, domain decomposition strategies and parallel gradient-type iterative solution schemes have been developed and implemented with success for 3-D Rayleigh-Benard-

Marangoni flow calculations [2]. These techniques permit making fundamental phenomenological flow studies at the grid resolution necessary to represent the fine scale surface-driven phenomena. Several adaptive timestepping selection strategies have been also studied as a means to provide stable accurate transient (and steady state) solutions more efficiently [18, 20].

Our main objective in the present work is to study and to implement numerical and computational techniques capable of improving the computational efficiency of algorithms for solving 2D coupled viscous flow and heat transfer computations. Our contribution will be in the direction of reducing the total computational effort using an adaptive timestep selection algorithm coordinated with control strategies for iterative solution of nonlinear equations in ODE solvers, and also partitioned analysis procedures for coupled systems. The nonlinear systems are solved by an inexact Newton method with iterative solutions of the linear systems at each step. We also want to perform phenomenological flow studies for monitoring the behavior of the fluid when time progress for different parameters of the Rayleigh-Benard-Marangoni problem.

The equations describing 2D Rayleigh-Benard-Marangoni flows are the coupled incompressible Navier Stokes and heat transfer equations. The present algorithm employs a decoupled scheme, where the momentum and continuity equations are solved first, in each timestep, lagging the temperature in the forcing term. Then, the heat transfer equation is solved with the computed velocities as input. The finite element flow formulation is based on a penalty Galerkin method to enforce the incompressibility constraint, and the heat equation utilizes a Galerkin approach. Spatial discretization of the Navier Stokes equations gives rise to a semi-discrete ODE system for the velocities that are usually solved by an implicit method. An adaptive timestep selection scheme is central to an efficient numerical integration of the ODE equations. At each timestep, a system of nonlinear equations has to be solved. It is common practice to use fixed-point iterations or Newton iterations. Since the convergence rate of such methods depends on the timestep, algorithms for an efficient solution should interact with the timestep selection strategies. It is necessary to coordinate these strategies so that efficiency is maintained. Gustafsson and Söderlind, [12], developed convergence control algorithms for handling the iterative solution of nonlinear equations in ODE solvers coordinated with adaptive timestep selection strategies.

Iterations of Newton's method requires the solution of linear systems, and iterative methods are typically preferred to this. Since we do not need to ob-

tain exact solutions of these systems, the appropriate method is an inexact Newton method [17, 14]. The accuracy required in solving the linear systems varies as the nonlinear algorithm proceeds, and this accuracy requirement uses nonlinear residual information. This scheme often strongly improves computational time and in some cases can improve robustness. The use of iterative solvers allows us to solve more practical applications related to the Rayleigh-Benard-Marangoni problem. However, iterative solvers tend to present a poor performance in penalty formulations basically due to the ill-condition introduced by the penalty parameter. To overcome this difficulty we are using them in the context of inexact Newton methods, where the initial solution of the nonlinear system are usually obtained with few iterations of the linear solver. The preconditioned Generalized Minimum Residual (GMRES) method is a Krylov-subspace method design to solve nonsymmetric linear systems [14]. Although there is no clear best Krylov subspace method, preconditioned GMRES is a very attractive method for this class of problem. The GMRES convergence is smooth and the overall algorithm is very easy to implement. Potential bottlenecks are preconditioning computations and matrix-vector products. Element-by-element preconditioners and matrix-vector products will be used, saving memory and speeding our computations.

The last consideration in this study is the use of partitioned analysis procedures for coupled systems. In the partitioned solution approach, the system is broken down into partitions in accordance with the physical and computational characteristics. The solution is separately advanced in time over each partition that, in our case, are the flow and heat calculations. Interaction effects need to be accounted for periodical transmission and synchronization of the coupled variables, velocities and temperature.

The outline of the treatment is as follows. In the next chapter we state the equations of the 2D Rayleigh-Benard-Marangoni problem, the finite element formulation, and solution approach. Next, we show validation test problems for steady state solutions of the classic Rayleigh-Benard problem for different values of the Rayleigh number. We also study problems involving the effect of the thermocapillary force at the free surface for different values of the Marangoni number. Last, we present the approach we are going to use in the thesis.

Chapter 2

Results

2.1 Rayleigh-Benard-Marangoni flows

2.1.1 Formulation and Approximation

We consider the transient flow of viscous incompressible fluid as described by the Navier-Stokes equations coupled to the heat transfer (energy) equation. The effect of buoyancy is included as temperature dependent body force term in the momentum equations by means of the Boussinesq approximation [11]. The applied temperature field induces a surface tension equivalent to the application of a shear stress at the horizontal free surface. The velocity field enters the convective term in the heat transfer equation.

The Navier Stokes equations for viscous flow of incompressible fluid may be written as

$$\frac{\partial \mathbf{u}}{\partial t} + \mathbf{u} \cdot \nabla \mathbf{u} - \nu \Delta \mathbf{u} + \frac{1}{\rho} \boldsymbol{\nabla} p = -\beta (T - T_0) \mathbf{g} \quad \text{in } \Omega \tag{2.1}$$

$$\boldsymbol{\nabla} \cdot \mathbf{u} = 0 \quad \text{in } \Omega \tag{2.2}$$

where $\mathbf{u}$ is the velocity, p is the pressure, Ω is the flow domain, T is the temperature, T_0 is the reference temperature, ν is the kinematic viscosity, ρ is the density, β is the thermal coefficient, and $\mathbf{g}$ is the gravity vector. We assume that there is no slip at the solid walls $\partial\Omega_1$, i.e., $\mathbf{u} = \mathbf{u_w}$ where $\mathbf{u_w}$ is the specified wall boundary velocity. The Marangoni problem involves a shear stress boundary in $\partial\Omega_2$. The surface stress, τ_{fb}, tangent to the free

boundary is equal to the gradient in the surface tension σ,

$$\tau_{fb} = \mu \frac{\partial u}{\partial y} = \frac{\partial \sigma}{\partial x} = \sigma_T \frac{\partial T}{\partial x} \tag{2.3}$$

where $\sigma_T = \frac{\partial \sigma}{\partial T}$ is determined empirically for a given fluid. We assume here that σ varies linearly with T, so σ_T is a constant for a given fluid.

The temperature of the fluid is governed by the energy transport equation for negligible viscous dissipation

$$\rho c_p \frac{\partial T}{\partial t} + \rho c_p \mathbf{u} \cdot \nabla T - \nabla \cdot (k \nabla T) = 0 \quad \text{in } \Omega \tag{2.4}$$

where $\mathbf{u}$ is the velocity, ρ is the density, c_p is the specific heat, and k is the thermal conductivity. Temperature, flux or mixed thermal boundary conditions may be applied.

The equations are scaled as follows: $x^*; y^* = x; y\frac{1}{L}$, $t^* = \frac{t\nu}{L^2}$, $u^*; v^* = u; v\frac{L}{\nu}$, $T^* = \frac{T - T_0}{\Delta T}$ where ΔT is a scaling factor, and $p^* = (\frac{p}{\rho})\frac{L^2}{\nu^2}$. Substituting these relations into (2.1), (2.2) and (2.4), we obtain the dimensionless formulation of the equations

$$\begin{aligned} \frac{\partial \mathbf{u}}{\partial t} + \mathbf{u} \cdot \nabla \mathbf{u} - \Delta \mathbf{u} + \boldsymbol{\nabla} p &= -\frac{Ra}{Pr} T \mathbf{g} && \text{in } \Omega && (2.5) \\ \boldsymbol{\nabla} \cdot \mathbf{u} &= 0 && \text{in } \Omega && (2.6) \\ \frac{\partial T}{\partial t} + \mathbf{u} \cdot \nabla T - \frac{1}{Pr} \nabla^2 T &= 0 && \text{in } \Omega && (2.7) \end{aligned}$$

where we dropped the superscript * for simplicity. The non-dimensional constants are: the Rayleigh number $Ra = \frac{\beta \Delta T g L^3}{\nu \alpha}$ and the Prandtl number $Pr = \frac{\nu}{\alpha}$, where $\alpha = \frac{k}{\rho c_p}$ is the thermal diffusivity. The boundary condition on the free surface (2.3) becomes

$$\frac{\partial u}{\partial y} = \frac{Ma}{Pr} \frac{\partial T}{\partial x} \tag{2.8}$$

where $Ma = \frac{\sigma_T \Delta T L}{\rho \nu \alpha}$ is the Marangoni number. Equations (2.5), (2.6) and (2.7) constitute a coupled system of equations to be solved for velocity, pressure and temperature.

The present algorithm employs a decoupled scheme, where the Navier-Stokes equations are solved first, in each timestep, lagging the temperature

in the forcing term. Then the temperature is calculated, with the velocities as input. The finite element flow formulation is based on a penalty Galerkin method to enforce the incompressibility constraint, and the heat equation utilizes a Galerkin approach.

We now consider the following penalized variational formulation of the Navier-Stokes equation [4]: for $\epsilon > 0$, find $\mathbf{u}^\epsilon \in V$ satisfying the initial condition with $\mathbf{u}^\epsilon = \mathbf{u_w}$ on $\partial\Omega_1$ such that

$$\begin{aligned}\int_\Omega (\frac{\partial \mathbf{u}^\epsilon}{\partial t} \cdot \mathbf{v} \;&+\; \nabla \mathbf{u}^\epsilon{:}\nabla \mathbf{v} \;+\; (\mathbf{u}^\epsilon \cdot \nabla)\mathbf{u}^\epsilon \cdot \mathbf{v}^\epsilon \;+\; \frac{1}{2}(\nabla \cdot \mathbf{u}^\epsilon)(\mathbf{u}^\epsilon \cdot \mathbf{v}) \\ &+\; \frac{1}{\epsilon}(\nabla \cdot \mathbf{u}^\epsilon)(\nabla \cdot \mathbf{v}))\, dx \;+\; \int_{\partial\Omega_2} \frac{Ma}{Pr} \nabla T \cdot \mathbf{v} ds \\ &=\; -\int_\Omega \frac{Ra}{Pr} T\mathbf{g} \cdot \mathbf{v}\, dx \end{aligned} \tag{2.9}$$

for all admissible $\mathbf{v} \in V$ with $\mathbf{v} = \mathbf{0}$ on $\partial\Omega_1$. The pressure approximation for the penalty formulation follows as

$$p^\epsilon = -\frac{1}{\epsilon} \nabla \mathbf{u}^\epsilon \tag{2.10}$$

where $\mathbf{u}^\epsilon$ is the solution to the penalty problem. Observe that the term $\frac{1}{2}(\nabla \cdot \mathbf{u}^\epsilon)(\mathbf{u}^\epsilon \cdot \mathbf{v})$ we have added to ensure coercivity reduces to zero when $\nabla \cdot \mathbf{u} = 0$. As $\epsilon \to 0$, $\mathbf{u}^\epsilon$ will converge to the velocity $\mathbf{u}$ and p^ϵ will converge to the pressure p. For a discussion of existence and uniqueness see, e.g., [4, 3].

Consider now approximation of the variational problem (2.9) using finite elements. Let $V^h \subset V$ be the finite element approximation space for velocities. In the usual way, the flow domain Ω is discretized to a union Ω_h of elements Ω_e, e = 1,2,. . . ,E. Lagrange piecewise polynomials are used as global basis functions ϕ_j, j = 1,2,. . . ,N, for the approximate subspace V^h. In this study we use continuous piecewise bilinear and piecewise biquadratic basis functions defined on a uniform discretization Ω_h of rectangular elements.

The direct approximation of the penalized variational problem (2.9) is to find $\mathbf{u}_h \in V^h$ satisfying the initial condition with $\mathbf{u}_h = \mathbf{u}_w$ on $\partial\Omega_1$ such that

$$\begin{aligned}\int_{\Omega_h} (\frac{\partial \mathbf{u}_h}{\partial t} \cdot \mathbf{v}_h \;&+\; \nabla \mathbf{u}_h{:}\nabla \mathbf{v}_h \;+\; (\mathbf{u}_h \cdot \nabla)\mathbf{u}_h \cdot \mathbf{v}_h \;+\; \frac{1}{2}(\nabla \cdot \mathbf{u}_h)(\mathbf{u}_h \cdot \mathbf{v}_h) \\ &+\; \frac{1}{\epsilon}(\nabla \cdot \mathbf{u}_h)(\nabla \cdot \mathbf{v}_h))\, dx \;+\; \int_{\partial\Omega_{2h}} \frac{Ma}{Pr} \nabla T \cdot \mathbf{v}_h ds \\ &=\; -\int_{\Omega_h} \frac{Ra}{Pr} T\mathbf{g} \cdot \mathbf{v}_h\, dx \quad \text{for all } \mathbf{v}_h \in V^h \end{aligned} \tag{2.11}$$

with pressure approximation given by

$$p_h = -\frac{1}{\epsilon}\nabla \mathbf{u}_h. \tag{2.12}$$

Introducing the discretization of elements and the basis functions, the velocities are

$$u_{sh}(\mathbf{x}) = \sum_{j=1}^{N} u_j^s \phi_j(\mathbf{x}), \tag{2.13}$$

where s is the velocity component index (s = 1,2 for 2D flow) and $\mathbf{u}^s$ is the nodal vector. Using $\boldsymbol{\omega}_h = (\phi_i, 0)$ and $(0, \phi_i)$ at interior node i, we have the following non-linear semidiscrete system of ordinary differential equations

$$\bar{\mathbf{M}}\frac{d\mathbf{u}^*}{dt} + \bar{\mathbf{A}}\mathbf{u}^* + \mathbf{C}(\mathbf{u}^*) + \frac{1}{\epsilon}\bar{\mathbf{B}}\mathbf{u}^* = \bar{\mathbf{F}} \tag{2.14}$$

where $\mathbf{u}^* = (\mathbf{u}^1, \mathbf{u}^2)^T$ and

$$\bar{\mathbf{M}} = \begin{bmatrix} \mathbf{M} & \mathbf{0} \\ \mathbf{0} & \mathbf{M} \end{bmatrix} \quad \bar{\mathbf{A}} = \begin{bmatrix} \mathbf{A} & \mathbf{0} \\ \mathbf{0} & \mathbf{A} \end{bmatrix} \quad \bar{\mathbf{B}} = \begin{bmatrix} \mathbf{B}_x & \mathbf{B}_{xy} \\ \mathbf{B}_{xy}^T & \mathbf{B}_y \end{bmatrix} \quad \bar{\mathbf{F}} = \begin{bmatrix} \mathbf{F}_x \\ \mathbf{F}_y \end{bmatrix}$$

with

$$\begin{aligned}
m_{ij} &= \int_{\Omega_h} \phi_i \phi_j \, dx \\
a_{ij} &= \int_{\Omega_h} ((\phi_i)_x (\phi_j)_x + (\phi_i)_y (\phi_j)_y) \, dx \\
(b_x)_{ij} &= \int_{\Omega_h} (\phi_i)_x (\phi_j)_x \, dx \\
(b_{xy})_{ij} &= \int_{\Omega_h} (\phi_i)_x (\phi_j)_y \, dx \\
(b_y)_{ij} &= \int_{\Omega_h} (\phi_i)_y (\phi_j)_y \, dx \\
(f_x)_i &= -\int_{\Omega_h} \frac{Ra}{Pr} T g_x \phi_i \, dx - \int_{\partial\Omega_{2h}} \frac{Ma}{Pr}\frac{\partial T}{\partial x}\phi_i \, ds \\
(f_y)_i &= -\int_{\Omega_h} \frac{Ra}{Pr} T g_y \phi_i \, dx - \int_{\partial\Omega_{2h}} \frac{Ma}{Pr}\frac{\partial T}{\partial y}\phi_i \, ds \\
\mathbf{C}(\mathbf{u}^*) &= \int_{\Omega_h} (\mathbf{u}_h \cdot \nabla)\mathbf{u}_h \cdot \mathbf{v}_h + \frac{1}{2}(\nabla \cdot \mathbf{u}_h)(\mathbf{u}_h \cdot \mathbf{v}_h) dx.
\end{aligned} \tag{2.15}$$

The nonlinearity resides in the convective term $\mathbf{C}(\mathbf{u}^*)$, which is linearized by successive approximations

$$\mathbf{C}(\mathbf{u}^*) \approx \mathbf{C}(\mathbf{u}^*_{k-1})\mathbf{u}^*_k = \int_{\Omega_h} (\mathbf{u}_{k-1} \cdot \nabla)\mathbf{u}_k \cdot \mathbf{v}_h dx \tag{2.16}$$

with initial iterates given by the solution at the previous step. Substituting (2.16) into (2.14), we obtain a sequence of linear problems for $\mathbf{u}^*_k$ at iterate k. Given $\mathbf{u}^*_0$, for $k = 1,2,\ldots$, solve

$$\bar{\mathbf{M}}\frac{d\mathbf{u}^*_k}{dt} + (\bar{\mathbf{A}} + \bar{\mathbf{C}} + \frac{1}{\epsilon}\bar{\mathbf{B}})\mathbf{u}^*_k = \bar{\mathbf{F}} \tag{2.17}$$

where

$$\bar{\mathbf{C}} = \begin{bmatrix} \mathbf{C} & \mathbf{0} \\ \mathbf{0} & \mathbf{C} \end{bmatrix}$$

with

$$c_{ij} = \int_{\Omega_h} \mathbf{u}_{k-1} \cdot \nabla\phi_j \, \phi_i \, dx.$$

The semidiscrete system (2.17) is integrate implicitly using a Crank-Nicolson scheme with timestep $\triangle t$,

$$\bar{\mathbf{M}}\frac{\mathbf{u}^*_{n+1,k} - \mathbf{u}^*_{n,k}}{\Delta t} + (\bar{\mathbf{A}} + \bar{\mathbf{C}} + \frac{1}{\epsilon}\bar{\mathbf{B}})\frac{\mathbf{u}^*_{n+1,k} + \mathbf{u}^*_{n,k}}{2} = \frac{\bar{\mathbf{F}}_{\mathbf{n+1}} + \bar{\mathbf{F}}_{\mathbf{n}}}{2} \tag{2.18}$$

where n denotes the time index. At each timestep we have to solve a sequence of linear systems of the form

$$\mathbf{P}\mathbf{u}^*_{n+1,k} = \mathbf{d} \tag{2.19}$$

where

$$\begin{aligned} \mathbf{P} &= \bar{\mathbf{M}} + \frac{\triangle t}{2}(\bar{\mathbf{A}} + \mathbf{C} + \frac{1}{\epsilon}\bar{\mathbf{B}}) \\ \mathbf{d} &= (\bar{\mathbf{M}} - \frac{\triangle t}{2}(\bar{\mathbf{A}} + \mathbf{C} + \frac{1}{\epsilon}\bar{\mathbf{B}}))\mathbf{u}^*_{n,k} + \frac{\triangle t}{2}\,(\frac{\bar{\mathbf{F}}_{n+1} + \bar{\mathbf{F}}_n}{2}) \end{aligned}$$

with

$$c_{ij} = \int_{\Omega_h} \mathbf{u}_{n,k-1} \cdot \nabla\phi_j \, \phi_i \, dx.$$

The algorithm to find the approximate velocities $\mathbf{u}^*_{n+1}$, $n = 0, 1, 2, \ldots$, can be described as follows:

- Given $\mathbf{u}_0^*$, Δt, ϵ, k_{max}
- Repeat for $n = 0, 1, 2, \ldots$
  1. $\mathbf{v}_0 \leftarrow \mathbf{u}_n^*$
  2. $k = 1$, $err = \epsilon + 1$
  3. Repeat while $(err > \epsilon)$ and $(k < k_{max})$
     (a) Solve $P\mathbf{v}_k = d$ where

$$\begin{aligned} \mathbf{P} &= \bar{\mathbf{M}} + \frac{\triangle t}{2}(\bar{\mathbf{A}} + \mathbf{C} + \frac{1}{\epsilon}\bar{\mathbf{B}}) \\ \mathbf{d} &= (\bar{\mathbf{M}} - \frac{\triangle t}{2}(\bar{\mathbf{A}} + \mathbf{C} + \frac{1}{\epsilon}\bar{\mathbf{B}}))\mathbf{u}_n^* + \frac{\triangle t}{2}\,(\frac{\bar{\mathbf{F}}_{n+1} + \bar{\mathbf{F}}_n}{2}) \end{aligned}$$

     with

$$c_{ij} = \int_{\Omega_h} \mathbf{v}_{k-1} \cdot \nabla\phi_j \, \phi_i \, dx.$$

     (b) Calculate the $err = \frac{\|\mathbf{v}_k - \mathbf{v}_{k-1}\|}{\|\mathbf{v}_k\|}$
     (c) $\mathbf{v}_{k-1} \leftarrow \mathbf{v}_k$
     (d) $k = k + 1$
  4. $\mathbf{u}_{n+1}^* \leftarrow \mathbf{v}_k$
  5. $\mathbf{u}_n^* \leftarrow \mathbf{u}_{n+1}^*$

If the penalty term in (2.14) is integrated exactly then the method will not yield solutions $\mathbf{u}_h$ that converge to $\mathbf{u}$ as $\epsilon \to 0$. The velocity field $\mathbf{u}_h \to 0$ as $\epsilon \to 0$ and the constraint equation $\nabla \cdot \mathbf{u} = 0$ dominates in this limit. The discrete finite element solution is said to "lock" [see, e.g.,[22],[15],[13]]. To obtain an approximate solution other than the "locking" solution, we use reduced integration for evaluating the penalty integral. The penalty term is approximately integrated using a Gauss quadrature rule of lower order than that required for exact integration.

If we denote $I(\cdot)$ the reduced quadrature rule for the penalty integration, the penalty term in (2.14) is given by

$$\frac{1}{\epsilon}\bar{\mathbf{B}}\mathbf{u}^* = \frac{1}{\epsilon}\int_{\Omega_h} I\left((\nabla \cdot \mathbf{u}_k)\,(\nabla \cdot \mathbf{v}_h)\right)\, dx. \tag{2.20}$$

In the numerical studies we consider two special cases: continuous piecewise bilinear basis of the 4-node bilinear quadrilateral for approximating the velocities with one-point Gauss quadrature rule for the penalty term (2.20) and

continuous piecewise biquadratic basis of the 9-node biquadratic quadrilateral for approximating the velocities with (2×2) Gauss quadrature rule for the penalty term (2.20). The solution of the linear system (2.19) is obtained using a frontal solver.

To find approximate solutions for the transport problem corresponding to (2.7), we use a traditional Galerkin finite element formulation. A week variational statement may be obtained by integration by parts of the diffusion term in a standard residual formulation, and then using the Gauss divergent theorem. The variational problem reduces to solving for T satisfying the initial conditions such that

$$\int_{\Omega} (\frac{\partial T}{\partial t}\omega + \mathbf{u} \cdot \nabla T\, \omega + \frac{1}{Pr}\nabla T \cdot \nabla \omega)\, dx = 0 \tag{2.21}$$

for all admissible test functions $\omega \in H_0$.

Assuming that convective and diffusive effects are of same order, we may construct a semidiscrete Galerkin finite element method introducing a spatial discretization and an appropriate finite element space for the admissible functions in (2.21). Let Ω_h denote the finite element discretization of Ω, and $H_0^h \subset H_0$ be the finite-dimensional subspace spanned by finite element basis ψ_i, i = 1,2,. . . ,N. The finite element problem is to find $T_h \in {H_0}^h$ satisfying the initial condition such that

$$\int_{\Omega_h} (\frac{\partial T_h}{\partial t}\omega_h + \mathbf{u} \cdot \nabla T_h\, \omega_h + \frac{1}{Pr}\nabla T_h \cdot \nabla \omega_h)\, dx = 0 \tag{2.22}$$

for all $\omega_h \in {H_0}^h$. The finite element approximation for the temperature T_h at any time t can be expressed as

$$T_h(\mathbf{x}, t) = \sum_{j=1}^{N} T_j(t)\psi_j(\mathbf{x}) \tag{2.23}$$

where the nodal solution values T_j depend continuously on time. We have in this studies continuous piecewise basis functions defined by the 4-node bilinear quadrilateral, the 9-node biquadratic quadrilateral and the 6-node biquadratic triangle.

Introducing (2.23) into (2.22) and setting $\omega_h = \psi_i$, i = 1,2,. . . ,N, we have the resulting semi-discrete ODE system for the nodal vector $\mathbf{T}$

$$\mathbf{M}\frac{d\mathbf{T}}{dt} + \mathbf{B}(\mathbf{u})\,\mathbf{T} + \mathbf{D}\,\mathbf{T} = 0 \tag{2.24}$$

where

$$\begin{aligned} m_{ij} &= \int_{\Omega_h} \psi_i \psi_j \, dx \\ b_{ij} &= \int_{\Omega_h} \mathbf{u} \cdot \nabla \psi_j \psi_i \, dx \\ d_{ij} &= \int_{\Omega_h} \frac{1}{Pr} \nabla \psi_i \cdot \nabla \psi_j \, dx \end{aligned}$$

We integrate the ODE system implicitly using a Crank-Nicolson scheme with timestep $\triangle t$. We have to solve at each timestep $\triangle t$ a linear system of the form

$$\mathbf{F}(\mathbf{T}^{n+1}) = 0 \tag{2.25}$$

where

$$\mathbf{F}(\mathbf{T}^{n+1}) = (\mathbf{M} + \frac{\triangle t}{2}(\mathbf{B} + \mathbf{D}))\, \mathbf{T}^{n+1} \, + \, \mathbf{G}$$

with

$$\mathbf{G} = -\,(\mathbf{M} - \frac{\triangle t}{2}(\mathbf{B} + \mathbf{D}))\, \mathbf{T}^{n}$$

and n denotes the timestep index. The solution of the linear system (2.25) is obtained using a frontal solver.

2.1.2 Validation Studies

Our first example involves natural convection in a unit square with heated lateral walls and adiabatic top and bottom walls. We consider two flows with different Rayleigh number Ra to demonstrate the effect of the Rayleigh numbers on the flow. The computed Nusselt number at the left wall, Nu_0, and the stream function at the midpoint, ψ_{mid}, are compared to the results from [8, 10, 9] to validate our code.

Consider the two-dimensional flow of a Boussinesq fluid of Prandtl number 0.71 in an square cavity described by $0 \leq x, y \leq 1$. Both components of the velocity are zero on all the boundaries, the boundaries at $y = 0$ and 1 are insulated, $\frac{\partial T}{\partial y} = 0$, and $T = 1$ at $x = 0$ and $T = 0$ at $x = 1$. We calculate the flow and thermal field for Rayleigh numbers of 10^3 and 10^4. The Nusselt number expresses the ratio of convective heat transfer to diffusive heat transfer in the vicinity of a wall (boundary layer). For this studied case, the Nusselt number satisfies

$$Nu_0 = \int_0^1 q dy,$$

where q is the heat flux.

The approximate velocity and temperature are calculated using biquadratic elements and an uniform mesh with size $h = \frac{1}{16}$. The results are shown in Table (2.1), and the agreement for both Rayleigh numbers is good.

	Benchmark		Our solution	
Ra	Nu_0	ψ_{mid}	Nu_0	ψ_{mid}
10^3	1.117	1.174	1.118	1.174
10^4	2.238	5.071	2.258	5.047

Table 2.1: Comparison of specific results to benchmark case

The contours of the stream function and temperature at $Ra = 10^3$ and $Ra = 10^4$ are shown in Figures (2.1) and (2.2). These figures provide the essential feature of this type of flow, the fluid rising along the heated wall and sinking along the cooled wall. The temperature difference is the "engine" driving the flow. The temperature is convected in a clockwise manner from the pure conduction solution. The stream function contour shows the concentric nature of the streamlines.

The second numerical experiment involves buoyancy forces due to temperature gradients and thermocapillary forces caused by gradients in the surface tension. The flow domain and boundary conditions are the same as the first example except that the top is now a flat free surface. The Rayleigh number is 10^3 and the problem is solved at different Marangoni numbers.

First, at M = -1, the effect of the surface tension is small and the streamlines are roughly circular, see Figure (2.3). The solution is similar in structure to the classic buoyancy driven flow studied in the first example, Figure (2.1). The effect of the thermocapillary force at the free surface is more pronounced at M = -100, see Figure (2.4). The streamlines are concentrated near the top boundary. At M = -1000, the flow is being strongly driven at the top boundary as similar experiments presented in [21].

Now we consider the case where the surface tension is oppositely directed. Figure (2.5) shows the stream function contours for $M = 10$ and $M = 100$. The contours at $M = 10$ look similar to the solution at M = -1, Figure (2.3), due to the small thermocapillary effect. At $M = 100$, the surface tension effect is strong enough to reverse the flow on the top surface and two cells are formed.

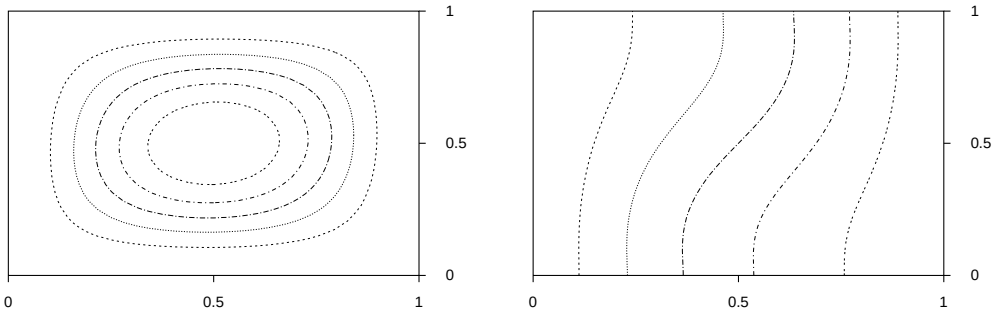

Figure 2.1: Stream function contour (left) and temperature contour (right) $Ra = 10^3$

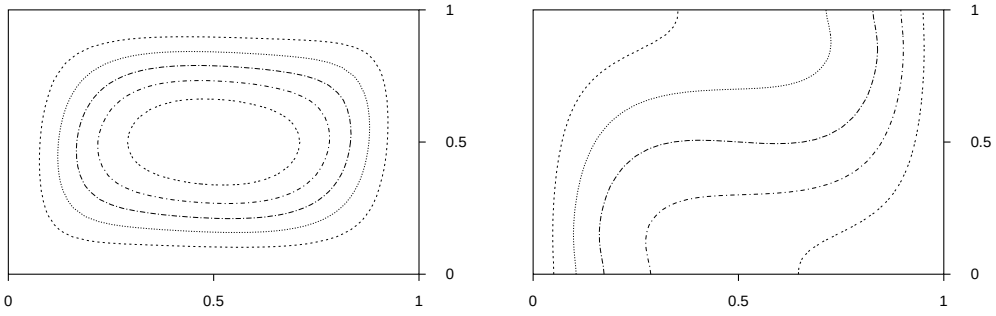

Figure 2.2: Stream function contour (left) and temperature contour (right) $Ra = 10^4$

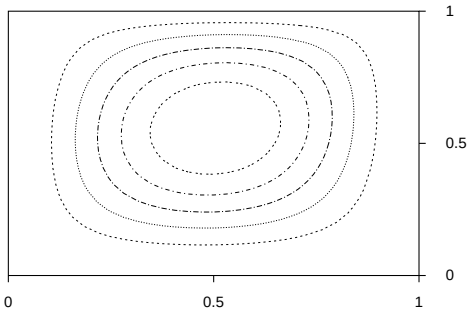

Figure 2.3: Stream function contours, $Ra = 10^3$ and $Ma = -1$

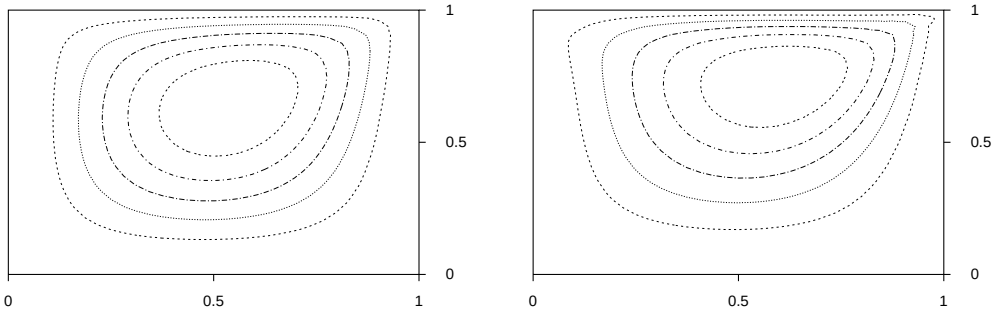

Figure 2.4: Stream function contours, $Ra = 10^3$, $Ma = -100$ (left) and Ma = -1000 (right)

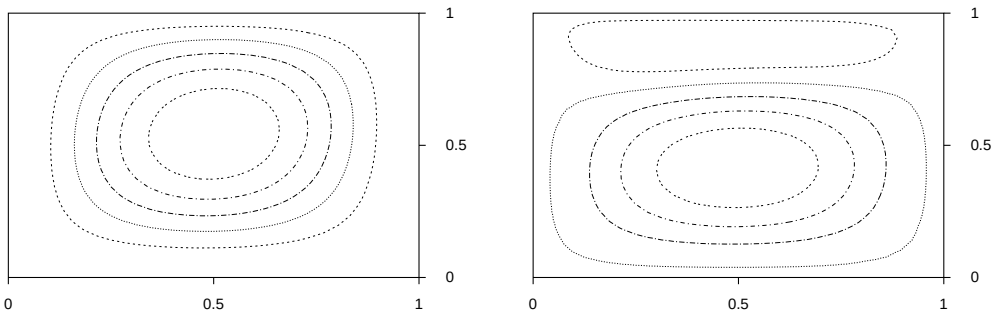

Figure 2.5: Stream function contours, $Ra = 10^3$, $Ma = 10$ (left) and $Ma = 100$ (right)

Chapter 3

Approach

The approach we are going to use in the thesis can be summarized in the following steps:

1. Implementation of the PID control algorithm for timestep selection as presented in [18] to solve coupled problems, like 2D Rayleigh-Benard-Marangoni flows.

2. Numerical experiments involving calculations of the kinetic energy for monitoring the liquid phase behavior when time progresses for Rayleigh-Benard problems [5, 7]. Then, expand the studies to include Marangoni effects.

3. Utilization of the nondimensional kinetic energy to improve timestep selection.

4. Study and implementation of control techniques for the iterative solution of nonlinear equations in ODE solvers [12].

5. Implementation of an iterative solver, the preconditioned GMRES, to find approximate solutions of the linear equations. At the moment, we have the linear systems solved by frontal elimination.

6. Implementation of an inexact Newton method to replace the successive approximation iterations used to find approximate solutions of the nonlinear systems.

7. Include partitioned analysis procedures for coupled systems to improve the efficiency of the calculations on the 2D Rayleigh-Benard problems [1].

8. Numerical studies of a practical problem where all the techniques can be applied and tested.

Bibliography

[1] C.A.Fellipa, K.-C. Park, and C. Farhat. Partitioned analysis of coupled systems. In *Proc. 4th World Congress on Computational Mechanics CD-ROM, CIMNE*, Barcelona, Spain, 1998.

[2] G.F. Carey, C. Harlé, R. Mclay, and S. Swift. Mpp solution of rayleigh-benard-marangoni flows. In *Supercomputing 97*, pages 1–13, San Jose, CA, 1997.

[3] G.F. Carey and R. Krishnan. Penalty finite element methods for the navier–stokes equations. *Comput. Meths. Appl. Mech. Engrg.*, 42:183–224, 1984.

[4] G.F. Carey and J.T. Oden. *Finite Elements: Fluid Mechanics*, volume 6. Prentice–Hall, Englewood Cliffs, NJ, 1986.

[5] G.F. Carey, W.B. Richardson, C.S. Reed, and B. Mulvaney. *Circuit, Device and Process Simulation - Mathematical and Numerical Aspects.* John Wiley & Sons, Chichester, England, 1996.

[6] B. M. Carpenter and G.M. Homsy. Combined buoyant-thermocapillary flow in a cavity. *J.Fluid Mech.*, 207:121–132, 1989.

[7] M.J. Crochet, F.T. Geyling, and J.J. Van Schaftingen. Finite element method for calculating the horizontal bridgman growth of semiconductor crystals. *Finite Elements in Fluids*, 6:321–337, 1985.

[8] G.De Vahl Davis. Laminar natural convection in a enclosed rectangular cavity. *Int.J. Heat Mass Transfer*, 11:1675–1693, 1968.

[9] G.De Vahl Davis. Natural convection in a square cavity: A comparison exercise. *Int.J.Num.Meth.Fluids*, 3:227–248, 1983.

[10] G.De Vahl Davis. Natural convection of air in a square cavity: A benchmark numerical solution. *Int.J.Num.Meth.Fluids*, 3:249–264, 1983.

[11] M. Griebel, T. Dornseifer, and T. Neunhoeffer. *Numerical Simulation in Fluid Dynamics - A Pratical Introduction*. SIAM, Philadelphia, PA, 1998.

[12] K. Gustafsson and G. Söderlind. Control strategies for the iterative solution of nonlinear equations in ode solvers. *SIAM J. Sci. Comput.*, 18(1):23–40, 1997.

[13] C. Johnson and J. Pitkaranta. Analysis of some mixed finite elements related to reduced integration. Technical report, Chalmers University of Technology and University of Göteborg, Göteborg, Sweden, 1980.

[14] C.T. Kelley. *Iterative Methods for Linear and Nonlinear Equations*. SIAM, Philadelphia, PA, 1995.

[15] D.S. Malkus and J.R. Hughes. Mixed finite element methods - reduced and selective integration techniques: A unification of concepts. *Comp. Meth. Appl. Mech. and Eng.*, 15:63–81, 1978.

[16] R.McLay and G.F. Carey. Coupled heat transfer and viscous flow, and magnetic effects in weld pool analysis. *Int. J. Numerical Methods Fluids*, 9:713–730, 1989.

[17] J.N. Shadid, R.S. Tuminaro, and H.F. Walaker. An inexact newton method for fully-coupled solution of the navier-stokes equations with heat and mass transport. Technical Report SAND97-0132, Sandia National Laboratories, Livermore, CA, 1997.

[18] A.M.P. Valli, G.F. Carey, and A.L.G.A. Coutinho. Finite element simulation and control of nonlinear flow and reactive transport. In *Proc. 10th Int. Conf. Finite Element in Fluids*, pages 450–455, Tucson, Arizona, 1998.

[19] D. Walgraef. *Spatio-Temporal Pattern Formation*. Springer-Verlag, New York, NY, 1997.

[20] J.M. Winget and T.J.R. Hughes. Solution algorithms for nonlinear transient heat conduction analysis employing element-by-element iterative strategies. *Comp. Meth. Appl. Mech. and Eng.*, 52:711–815, 1985.

[21] A. Zebib, G.M. Homsy, and E. Meiburg. High marangoni number convection in a square cavity. *Phys. Fluids*, 28(12):3467–3476, 1985.

[22] O.C. Zienkiewicz. *The Finite Element Method.* McGraw-Hill, U.K., 1977.